Nanoscale

Magnetic signatures of 120 K superconductivity at interfaces in $La_2CuO_{4+\delta}$

Journal:	*Nanoscale*
Manuscript ID	NR-ART-06-2019-004996.R1
Article Type:	Paper
Date Submitted by the Author:	04-Dec-2019
Complete List of Authors:	Choi, Eun Mi; University of Cambridge Department of Materials Science and Metallurgy Zhu, Bonan; University of Cambridge Department of Materials Science and Metallurgy Lu, Ping; Sandia National Laboratories, Feighan, John; University of Cambridge Department of Materials Science and Metallurgy Sun, Xing; Purdue University System, Materials Engineering Wang, Haiyan; Purdue University System, MSE; Neil Armstrong Engineering Building MacManus-Driscoll, Judith; University of Cambridge Department of Materials Science and Metallurgy

SCHOLARONE™
Manuscripts

Magnetic signatures of 120 K superconductivity at interfaces in $La_2CuO_{4+\delta}$

Eun-Mi Choi[1,], Bonan Zhu[1,*], Ping Lu[2], John Feighan[1], Xing Sun[3], Haiyan Wang[3], and Judith L. MacManus-Driscoll[1]*

1. Department of Materials Science & Metallurgy, University of Cambridge, 27 Charles Babbage Road, Cambridge, CB3 0FS, United Kingdom.

2. Sandia National Laboratories, Albuquerque, New Mexico 87185, United States.

3. Materials Engineering, Purdue University, West Lafayette, IN, 47907, United States.

Corresponding Author

*Correspondence: Dr. Eun-Mi Choi and Mr. Bonan Zhu, Department of Materials Science, University of Cambridge, 27 Charles Babbage Road, Cambridge, CB3 0FS, UK

E-mail: emc63@cam.ac.uk and bz240@cam.ac.uk

KEYWORDS: Superconductivity. Superconducting transition. Nanocomposite. Thin film.

Abstract

In self-assembled vertically aligned nanocomposite (VAN) thin films of $La_2CuO_{4+\delta}$ + $LaCuO_3$, we find from DC magnetic susceptibility measurements, weak signatures of superconductivity at ~ 120 K. This compares to a maximum T_C of 40 K in bulk $La_2CuO_{4+\delta}$. The 120 K signature occurs *only* when both *c*-axis *and a*-axis oriented $La_2CuO_{4+\delta}$ grains are both present in the films. The superconductivity was lost after 3 months of storage but was recovered by annealing in oxygen. From lattice parameter analyses undertaken close to the *c*/*a* grain boundaries, it was determined that expansion of the La perovskite block in *c*-$La_2CuO_{4+\delta}$ enables the differently oriented grains to join at the interface. This expansion is consistent with the higher T_C interfacial region. The work shows a new

direction for increasing T_C in cuprates - namely careful strain engineering of the crystal structure independently *in-plane* and *out-of-plane*.

Introduction

In all the cuprate superconductors (except electron-doped superconductors that do not have an apical oxygen, O_A, i.e. those with T'-structure) [1], a close relationship

between T_C and *out-of-plane* Cu-O_A distance has been clearly demonstrated in several different experimental studies, namely by chemical substitution of cations at adjacent sites [2–7], by applying hydrostatic pressure [8–12] and by controlling Madelung (electrostatic) potential [13–15]. Pavarini *et al.* calculated the correlations between T_C and hopping range which relates to the Cu-O_A distance [16] and showed that an extended Cu-O_A gives a larger hopping range and weaker contribution of the d_{z2} orbital of Cu. This in turn gives more localized conduction (more 2-D like) in the CuO_2 layers [16–20] which produces a higher T_C.

The $La_2CuO_{4+\delta}$ system is an ideal system to study for tuning Cu-O_A with the aim of increasing T_C. This is because it has a relatively low variation of excess oxygen content, i.e. $0.05 < \delta < 0.13$, and less likely to lose oxygen in response to strain as compared to some other cuprates, e.g. $YBa_2Cu_3O_{7-x}$. Plain films of $La_2CuO_{4+\delta}$ grown on a $LaSrAlO_4$ (LSAO, a = 3.755 Å) have a maximum T_C of ~ 30 K, which is lower than the maximum T_C of 40 K in bulk (for δ of 0.1 - 0.11) [14], and films on $SrTiO_3$ have a maximum T_C of only 11 K [21]. All $La_2CuO_{4+\delta}$ films need to be ozone annealed after growth to ensure optimal

doping via oxygen in interstitial positions [14]. In fact, while LSAO is an ideal substrate from a structural matching viewpoint, it is not ideal from a lattice size point of view as *a* = 3.755 Å is much smaller than the optimum ~ 3.84 Å value to achieve an optimum T_C [22–24].

T_C has been increased in $La_2CuO_{4+\delta}$ at interfacial regions, i.e. in 1-2 unit cell (u.c.), in epitaxial heterostructures, by stretching the Cu-O_A distance. Hence, in bilayer films of $La_{1.55}Sr_{0.45}CuO_4/La_2CuO_{4+\delta}$ (metal/superconductor layers) grown on LSAO, using Madelung strain T_C was increased to 50 K at the interface (from the bulk value of 40 K) by increasing the *c*-parameter (and hence also Cu-O_A distance) [13,14]. Further, by changing the substituent cation size on the A site in $La_{1.6}A_{0.4}CuO_4/La_2CuO_4$ (metal/insulator bilayer, with A = Ca, Sr, Ba) *both* dopant size and interface chemistry were shown to be important to superconductivity [5] with large cation size giving a larger cell and hence increased T_C owing to higher apical distance. However, in these metal/insulator bilayers T_C was shown to depend non-linearly on the *c*-parameter and it saturated at about 40 K. These aforementioned thin film studies confirmed earlier work

of uniaxial tensing (8 GPa) along the *c*-axis in $La_{1.85}Sr_{0.15}CuO_4$ single crystals which produced a T_C of 52 K [12]. Although not measured, the *c*-parameter (and Cu-O_A distance) would have increased under the uniaxial tensing.

Lattice strain is important not only to cuprate superconductors. In the FeSe system, an enhancement of T_C (to over 65 K from 8 K for the bulk material) was achieved [25–27] by growing epitaxial films on $SrTiO_3$ (STO). Both biaxial lattice strain and electronic structure reconstruction (by charge transfer from the oxygen-vacancy-induced states of the substrate) both appear to play a role in increasing T_C.

In this work, we do not use chemical substitution as this simultaneously expands (or contracts) *both* the *out-of-plane* (OOP) and *in-plane* (IP) lattice parameters. We also do not use substrate control of the *a*-parameter to induce an elastic expansion of the *c*-parameter (and hence Cu-O_A distance) since *c*-parameter and *a*-parameter cannot be controlled independently. Instead, we use a novel vertically aligned nanocomposite (VAN) approach.

In the designed structure, we aim to achieve vertical epitaxial growth of *c*-oriented $La_2CuO_{4+\delta}$ nanopillars (with ~ 10's nm dimension) within a $LaCuO_3$ matrix. Herein, $La_2CuO_{4+\delta}$ is referred to as 214 and $LaCuO_3$ as 113. Although detailed elastic moduli are not available for both 113 and 214, 113 is assumed to be stiffer than 214 along the *c*-direction because of the layered 214 structure should be more compliant along *c*-direction. Hence, the hypothesis is that 113 will dominate the strain state in 214 via vertical epitaxy. We note that *a*-parameter should be close to the bulk value because 214 does not grow coherently on STO, owing to the different lattice structures [21].

We chose 113 as a strain-controlling phase as it will not poison the 214 because it contains the same chemical constituents. In addition, since the 113 contains Cu^{3+}, it can act as an oxidizing source to dope the 214 [28]. Depending on its oxygen content, 113 has a rich magnetic phase diagram and various electric properties [29]. Under the film growth conditions, 113 will most likely to be in the composition range, $LaCuO_{3-\delta}$, $0 < \delta < 0.5$, which will make it antiferromagnet (AFM) [28–30]. We chose to study pure 214 and not $La_{1.85}Sr_{0.15}CuO_4$ ((Sr)214) because Sr would also substitute in the 113 that would lead

to sub-optimal, and more importantly, unspecified doping in 214. In our pure 214 system, optimal hole doping then relies on obtaining oxygenated 214.

Recently, we showed that T_C can be increased to 50 K at the 214/113 interfacial regions in composite films, these regions penetrating 10's nm into the 214. At the same time, reference plain 214 films on STO were *not* superconducting [31]. The superconductivity arose from vertical epitaxial tensing of the 214 by the 113 *without* reduction of the *a*-parameter [31].

In this work, in the same system 214/113 system, we compare films which either have or do not have some additional *a*-axis oriented 214 (*a*-214) oriented present in the films. Around half the films we grew had *a*-214 present in addition to *c*-axis oriented 214 (*c*-214). We study the difference in superconducting properties between films with and without the *a*-214 present. We find that *c*-214/*a*-214 boundaries are critical for observing the 120 K T_C phase. Lattice structure analyses from STEM images of the *c*-214/*a*-214 interfaces showed strong structural distortions of both the phases on either side of the boundary. Critically, highly strained structural units of *c*-214 *right at* the *c*-214/*a*-214

interfaces are observed. We propose a model to explain how the interfacial *c*-214 has a strongly expanded perovskite block, indicative of a strongly expanded Cu-O_A distance, and consistent with the presence of the higher T_C phase. The work shows the way to engineering higher *Tc* cuprates via 3D strain control.

Experimental

Three ceramic targets of La_2CuO_4, $LaCuO_3$, and $(La_2CuO_4)_2$:$(LaCuO_3)_3$ were synthesized by conventional solid-state reaction. First, a stoichiometric mixture of La_2O_3 and CuO was ground and subsequently calcined at 950 ^oC for 12 hours under oxygen flow. After cooling down the mixture to room temperature, it was ground again and this process was repeated three times. The mixture was ground and pressed into a pellet disk of about one inch in diameter. The pellet was sintered at 1050 ^oC for 12 hours under oxygen flow. TiO_2-terminated (001)-oriented $SrTiO_3$ (STO), 0.5 wt.% Nb doped $SrTiO_3$ (Nb:STO) (a = 3.905 Å) single crystal substrates (CrysTec GmbH) were used to grow the films on.

Epitaxial, self-assembled thin films of 214+113 were grown the $(La_2CuO_4)_2$:$(LaCuO_3)_3$ target, and plain reference films were grown from the La_2CuO_4 and $LaCuO_3$ targets using pulsed laser deposition (PLD). Films of ~ 30nm thickness were grown onto the TiO_2-terminated (001) STO substrates. A KrF excimer laser at a substrate temperature of 700 ^oC with a repetition rate of 2 Hz and a fluence of 1.2-1.5 J cm^{-2} with 0.13-0.14 mbar flowing O_2. After growth the films were annealed in 500 mbar O_2 at 500 ^oC for 60 minutes and then slowly cooled afterwards (at a rate of -10 ^oC/min) to room temperature, while maintaining 500 mbar O_2 background pressure.

The $(La_2CuO_4)_2$:$(LaCuO_3)_3$ target composition was chosen as opposed to any other ratio, in order to aimed to achieve relatively fine nanocolumns of *c*-axis oriented 214 (*c*-214), embedded in the 113 matrix. Since the *c*-parameter of bulk 113 (*c* = 3.97268 Å, *a* = 3.8189 Å) is most closely matched to the *a*-parameter of STO (*a* = 3.905 Å), in the films containing 113, it was expected that the 113 would grow with the *a*-axis OOP, giving *a*-axis oriented 113 films (*a*-113). Also, since 214 is structurally mismatched to

STO this means that the 214 will not grow coherently on the STO and so should be relaxed *in*-plane [21].

Magnetic property measurements were performed using a superconducting quantum interference device (SQUID, Quantum Design), in the temperature range of 10-250 K. Structural analysis of the films was done by X-ray diffraction (XRD) analysis using high resolution Panalytical Empyrean vertical diffractometer (Cu Kα radiation). An FEI Titan^{TM} G2 80-200 STEM with a Cs probe corrector, operated at 200 kV, was used in this study. The STEM images were recorded by using high-angle annular dark-field (HAADF) detector. Real space image analysis was used to obtain maps of lattice parameters. The open source package <Atomap> [32] was used to extract atomic column positions via fitting 2-D Gaussian functions. Pair-wise distances between neighboring columns were used to extract lattice parameters. Calibration was done using the distance between Sr columns in the STO substrate in the same field of view. The lattice parameter of STO was assumed to be 3.905 Å.

Results and discussion

Table 1. Details of films grown in this study compared to bulk 214

Sample no.	Substrate	Global Lattice Parameters of 214 (± 0.01 Å) from XRD	T_C & T_N
SREF214	STO	a = 3.81, c = 13.10	Non-superconducting
SREF113	STO	a = 3.90, c = 3.83 (113)	Non- superconducting
Bulk 214		a = 3.794, c = 13.1646	T_C = 40 K
S1	STO	a = 3.81, c = 13.14	T_C = 120 K (MT) T_N = ~60 K
S2	STO	a = 3.80, c = 13.14	T_C = 120 K (MT) T_N = ~60 K
S3	Nb:STO	a = 3.81, c = 13.14	T_C = 120 K (MT) T_N = ~60 K
S4	STO	a = 3.80, c = 13.13	T_C = 120 K (MT) T_N = ~60 K

Table 1 shows sample data from our study, with a focus on 4 films which showed magnetic signatures of 120 K superconductivity. None of the films were super-annealed to oxygenate (e.g. by ozone annealing). Rather they were just cooled in oxygen gas. We also show data for a plain reference 214 (S_{REF}214) film, plain 113 (S_{REF}113) and bulk 214. S_{REF}214 was non-superconducting, as expected, because again no excess

oxygen was supplied after growth, e.g. by ozone annealing, as is normally required for 214 [14,33,34]. S_{REF}113 was not superconducting, also as expected [28–30].

Fig. 1 shows the 113 film to be well (*h*00) aligned from X-ray diffraction (XRD), and to be antiferromagnetic (AFM), T_N ~ 50 K. The average OOP lattice parameter of S_{REF}113 measured from XRD was 3.83 ± 0.01 Å and the IP lattice parameter was 3.90 ± 0.01 Å, giving a cell volume of ~ 58.25 ± 0.01 Å^3. The structure is consistent with *a*-axis oriented tetragonal $LaCuO_{3-\delta}$, *a*-113 (bulk 113 has *a* = 3.8189 Å, *c* = 3.97268 Å, and u.c. volume 57.993 Å^3). The AFM properties are consistent with $0.03 < \delta < 0.16$, which is expected as the film was post-growth annealed under O_2 pressure of < 1 atm. [28–30].

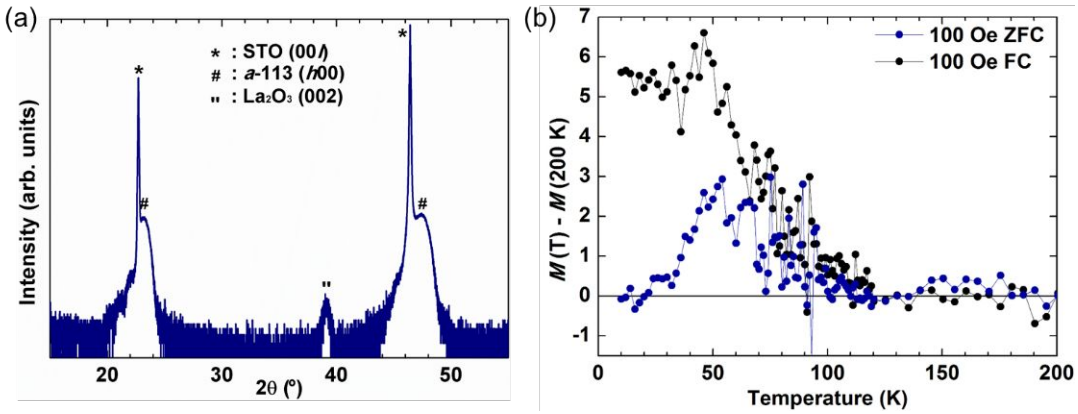

Fig. 1. XRD 2θ-ω spectra and *M (T)* for plain $LaCuO_3$ film (S_{REF}113). (a) XRD for $LaCuO_3$ film shows clear La113 with a small (002) La_2O_3 peak. (b) ZFC and FC

temperature dependence of the dimensionless magnetic moment curve, M(T)-M(200 K) at H = 100 Oe. It shows an AFM signal with T_N of ~ 60 K.

In the nanocomposite films (S1 – S4), the average OOP lattice parameters (from XRD and scanning transmission electron microscopy (STEM)) of a-113 are 3.81-3.83 Å which is again consistent with oxygen deficient 113 [30] and explains the AFM background observed in the magnetization versus temperature plots of the nanocomposite films, as shown later in Fig. 2 [29].

The global lattice parameters of 214 did not show any clear trend with T_C. The values on STO were all in the range a = 3.79 - 3.81 Å, c = 13.12 - 13.14 Å. The a-parameters are slightly larger than the bulk value of 214 (a = 3.794 Å), possibly because of a partial strain effect from the STO substrate. The c-parameters are all lower than the bulk 214 (13.1646 Å), possibly owing to the Poisson effect (moderate stretching of a-parameter will reduce c-parameter). We show later that *local* lattice parameters in 214 at interface regions in the film are markedly different to the average global lattice parameters, and are consistent with the enhanced T_Cs reported in Table 1.

In films S1 – S4, from the onset of the diamagnetic Meissner signal we observed weak magnetic transitions (~ 10^{-6} e.m.u., corresponding to up to ~ 2 % volume fraction of superconductor at 10 K), indicating a T_C up to 120 K (see supplementary information Fig. S1). This Meissner signals of is clearly shown by comparing to bare substrate (see supplementary information Fig. S2). To show the Meissner signal clearly, fig. 2(a) shows the ZFC M(T) at H = 100 Oe for film S1 solely. We could not observe an *in*-plane

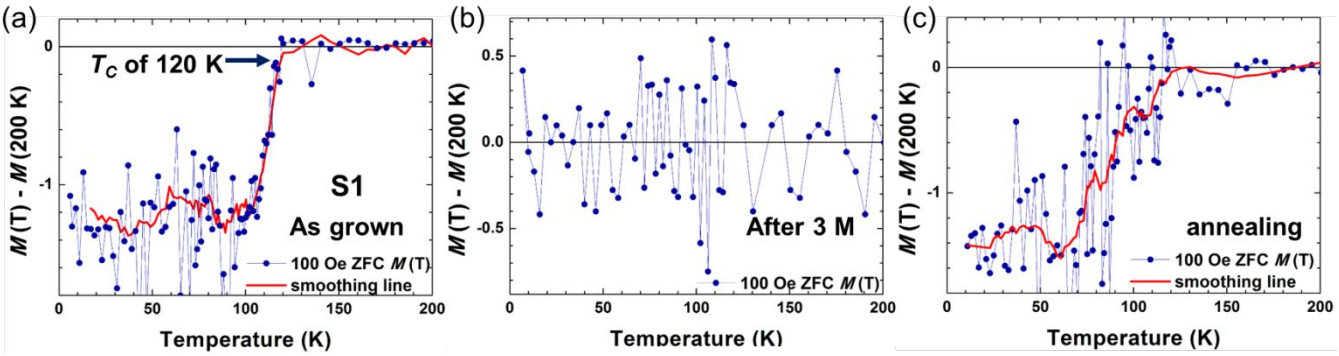

superconductive resistive transition in the films, either in a planar or top-to-bottom configuration (on conducting Nb-STO substrates). This is understood from the electron microscopy analysis that we show later: the superconductivity arises at interfaces and does not permit a connected superconducting path.

Fig. 2. Magnetic signatures of ~ 120 K superconductivity in 214 nanocomposite films.

ZFC temperature dependence of dimensionless magnetic moment, M(T) – M(200 K): (a) As-grown nanocomposite film showing T_C of ~ 120 K. (b) M(T) – M(200 K) after 3 months, showing that the superconducting Meissner signal disappeared. (c) M(T) – M(200 K) after annealing the film of b) at 400 ^{o}C under flowing O_2 gas for 2 hours. It is observed that the superconductivity is recovered.

An AFM transition at ~ 60 K was also observed in films S1-S4, consistent with the presence of oxygen-deficient 113 [29], similar to what was measured in the pure 113 film, S_{REF}113, of Fig. 1(b). After 3 months, the diamagnetic Meissner signal with 120 K onset disappeared (Fig. 2(b), Film S1). Fig. 2(c) shows the recovery of superconductivity after annealing at 400 ^{o}C for 2 h. under flowing O_2 gas, although the transition was slightly broadened. This disappearance and then reappearance of superconductivity is indicative of oxygen loss from some of the interstitial sites over time, followed by refilling of these sites. Oxygen loss from cuprate films over time is well known[35]. Furthermore, the activation energy for oxygen diffusion via interstitials is very low in Ruddelsden-

Popper phases[36]. The low activation energy for oxygen diffusion, the possible additional strain-enhanced oxygen diffusion, and the short diffusion distances (thin films with vertical interface diffusion paths) explain the oxygen loss over time. Since the films require an excess oxygen to be superconducting, oxygen loss will lead to a loss of superconductivity.

Fig. 3(a) shows a schematic of the crystal structure of 214. All films showed highly *c*-axis oriented 214 peaks (Film S2 is shown in Fig. 3(b)). To investigate the origin of this weak signature of higher T_C superconductivity in 214, we compared XRD data for films that showed the 120 K onset (Fig. 3(c)) to those that showed low T_Cs (<50 K) or no superconductivity (Fig. 3(d)). We find that the higher T_C films (Fig. 3(c)) show clear *a*-214 peaks whereas the films with no superconductivity or low T_C did not show obvious *a*-214 peaks. It is noted that *a*-214 is *not* present in the S_{REF}214 films.

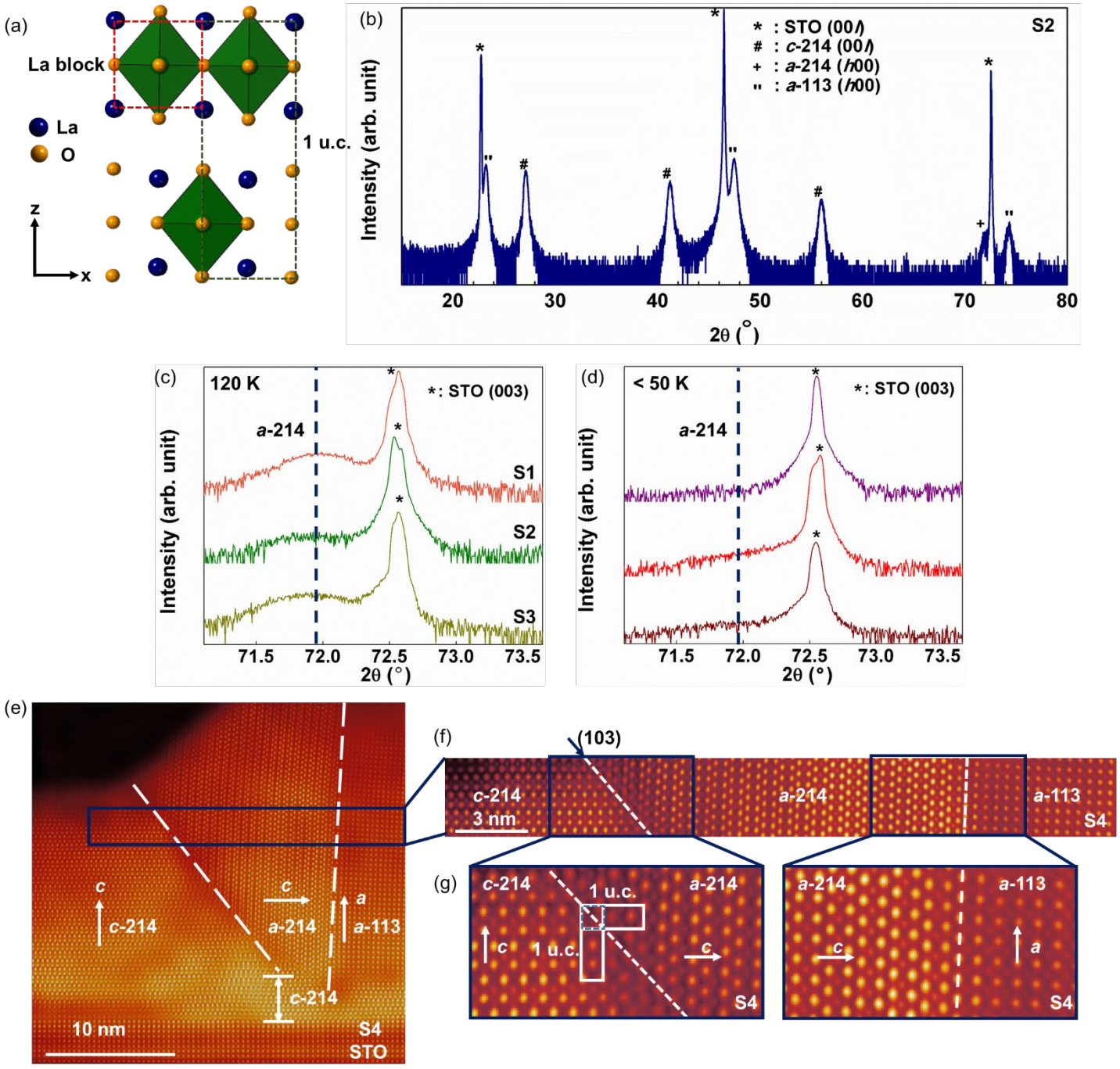

Fig. 3. Global and local structural information of nanocomposite films. (a) Two unit cells of 214 with the La pseudo-cubic block (red dashed lines) shown in one of the u.c. of 214 (green dashed lines). The CuO_6 octahedra are shown but not the individual Cu atoms.

(b) XRD 2θ-ω spectra of film S2 showing coexistence of *c*-214 and *a*-113 with a small amount of *a*-214. (c) XRD 2θ-ω spectra near the (003) STO peak for films which show weak magnetic signatures of 120 K superconductivity (films S1, S2 and S3). A small fraction of *a*-214 is present in these films. (d) XRD 2θ-ω spectra near the (003) STO peak for films which show no (or very minor) *a*-214 signatures of 120 K superconductivity. These films showing no superconductivity or low Tc (<50 K). (e) and (f) High-resolution STEM images of *c*-214/*a*-214 interface and *a*-214/*a*-113 interface. The white dashed lines indicate crystal boundaries between the different phases. Fig. 3(f) shows a magnified STEM image within the blue box in Fig. 3(e). (g) Highly-magnified STEM images showing clean and coherent interfaces both at the *c*-214/*a*-214 boundary (left) and at the *a*-214/*a*-113 boundary (right). The u.c.s of *c*-214 and *a*-214 are outlined by white solid line. The La pseudo-cubic perovskite block in 214 is also outlined by a blue dashed line.

Hence, it is found that the 120 K transition is NOT present in the samples with *a*-214 absent. The results indicate that the higher T_C material is related to the presence of *a*-

214. Also, it is noted that *a*-214 is only present in the composite and this is because it is epitaxially stabilized by the *a*-113 columns, as discussed in more detail below.

To learn more about the origin of the superconductivity in the films, a high-resolution STEM images which contains the 3 different phases in the film: *c*-214, *a*-214, and *a*-113, and the intersections of these phases was studied. For purposes of clarity, we show this same image three times (in Fig. 3(e), 4(a) and 5(a)) with a different focused region (and hence different labelling) for each figure. One region (Fig. 3(e)) was probing the quality of all the interfaces present. Another region (Fig. 4(a)) was studied for determination of the *out-of-plane* lattice parameter changes across the *a*-214/*a*-113 interface, to help understand why the *a*-214 is formed. A final region (Fig. 5(a)) was studied for determining the *in-plane* and *out-of-plane* lattice parameters across the *c*-214/*a*-214 interface, and hence to learn whether structural distortion at this interface can explain the observed superconductivity.

The high magnification HRSTEM images of the *c*-214/*a*-214 and *a*-214/*a*-113 interfaces (Fig. 3(f) and (g)) show the very high epitaxial quality and perfection of both

interfaces. The *c*-214/*a*-214 grains meet at a (103) interface (left image), similar to a twin boundary. The lowest energy *c*-214/*a*-214 interface will be formed by sharing of the perovskite blocks (outlined by blue dashed line, within the white oblong unit cells as show in Fig. 4(g)). We note that the *c*-214/*a*-214 boundaries do not penetrate all the way to the substrate surface. Instead, a *c*-214 layer forms the first layer of ~ 4nm thick on top of the STO substrate.

To understand more about the nature of the *c*-214/*a*-214 boundary and to confirm whether or not the 120 K superconductivity originates here or whether it could originate that at *a*-214/*a*-113 boundary, we need to consider the *a*-214 structure, which will be influenced by its vertical epitaxial growth on the majority *a*-113 phase. The question is why is *a*-214 stabilized and what are the details of its structure.

First, we observe that the *a*-214/*a*-113 grains meet along a (010) boundary (Fig, 4(a)). The lowest energy interface will be if the grains share the La perovskite blocks again, just as for the *c*-214/*a*-214 boundaries. We note that Fig. 4(a) is the same STEM image of Fig. 3(e) but now with horizontal lines drawn (A to B) to indicate the regions where

lattice parameter analyses were undertaken, and the vertical lines are drawn to indicate the extent of the vertical regions over which the lattice parameters were averaged.

The *a*-parameter was measured to be ~3.95 ± 0.01 Å in the *a*-124/*a*-113 interfacial region (Fig. 4(b)). This lattice parameter corresponds to the non-superconducting T'214 phase. Hence, this interface *cannot* be the origin of the 120 K superconductivity. Nevertheless, the interface was of very high quality and continuous lattice parameter variation was observed across it with lattice matching at the interface (*a*-113 was stretched compared to bulk, and T'*a*-214 was compressed compared to bulk).

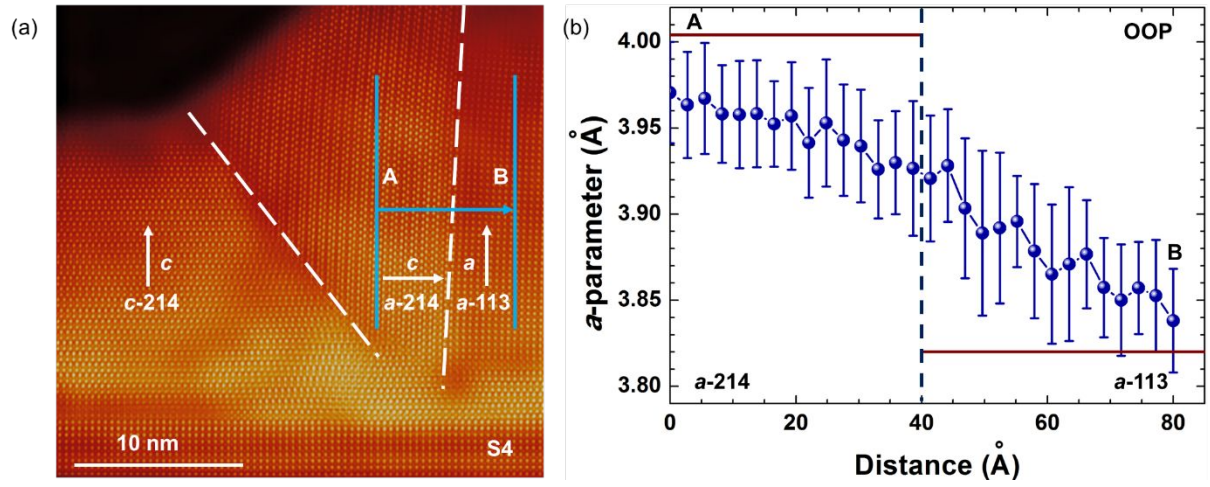

Fig. 4. Lateral variation of *a*-parameters (OOP direction) across the *a*-214/*a*-113 interface. (a) The blue arrow from point A to B shows the horizontal distance over which

the lattice parameters were analyzed. (b) Measured *a*-parameters. Brown lines show *a*-parameters for bulk T'214 (left hand side of image) and bulk *a*-113 (right hand side of image).

Further confirmation of the fact that the *a*-214 grains had the T'214 structure was made by measuring the LaO spacer layers in the *a*-214 grains. The value was found to be ~ 2.50 Å, which corresponds to the T'-structure. In *c*-214, the spacer layer distance is 2.95 Å [1]. T'214 is not superconducting because electron doping is essential for superconducting T'214 [37]. Bulk T'214 has $a \sim 4.0$ Å and $c \sim 12.3$-12.5 Å, depending on the oxygen content [38,39], whereas the standard tetragonal 214 phase (T214), as observed in the *c*-214 grains, has $a = 3.794$ Å and $c = 13.1646$ Å. The essential difference between the T and T' structures is that apical oxygen is present in the former but not in the latter [1,38,39].

The T'214 structure formation is consistent with a compression of the *a*-214 grains along the IP direction, and is explained by the location of the grains. They form *between* the upwardly growing (and impinging) *c*-214 and *a*-113 grains. Hence, the *a*-214 grains

will be laterally squeezed between the *c*-214 and *a*-113 grains. We note that in bulk, substitution of smaller Y for La into 214 gives T'214 instead of T214 [40] as a result of chemical compression. We have a similar effect here, but with mechanical pressure instead of chemical pressure.

As already noted, superconductivity with T_C of ~ 120 K cannot originate from the T'214 phase itself. Since we already showed that *a*-214 must be present in order to observe the 120 K transition and since the superconductivity cannot originate in the a-214 because it has the T' structure, it must originate in the *c*-214 grains at the *c*-214/*a*-214 interface. We now explore the lattice parameters in the region of the *c*-214/*a*-214 interface to determine whether a highly strained interfacial structure could be present and hence be responsible for the enhanced T_C.

We now focus on the lattice parameters of *c*-214/*a*-214 interfaces, and hence the HRSTEM image is now shown with lines drawn (A-B and C-D) to indicate regions where lattice parameter analyses were undertaken (Fig. 5(a)). The slanted horizontal lines indicate the extent of the regions over which the lattice parameters were averaged. The

lattice parameters were analyzed to within 10 Å of the interface. In Fig. 5(b), we show the *c*-parameter (*a*-parameter) in *c*-214 (*a*-214) adjacent to the *a*-parameter (*c*-parameter) in *a*-214 (*c*-214), as these lie along the same direction, i.e. both perpendicular (parallel) to the substrate.

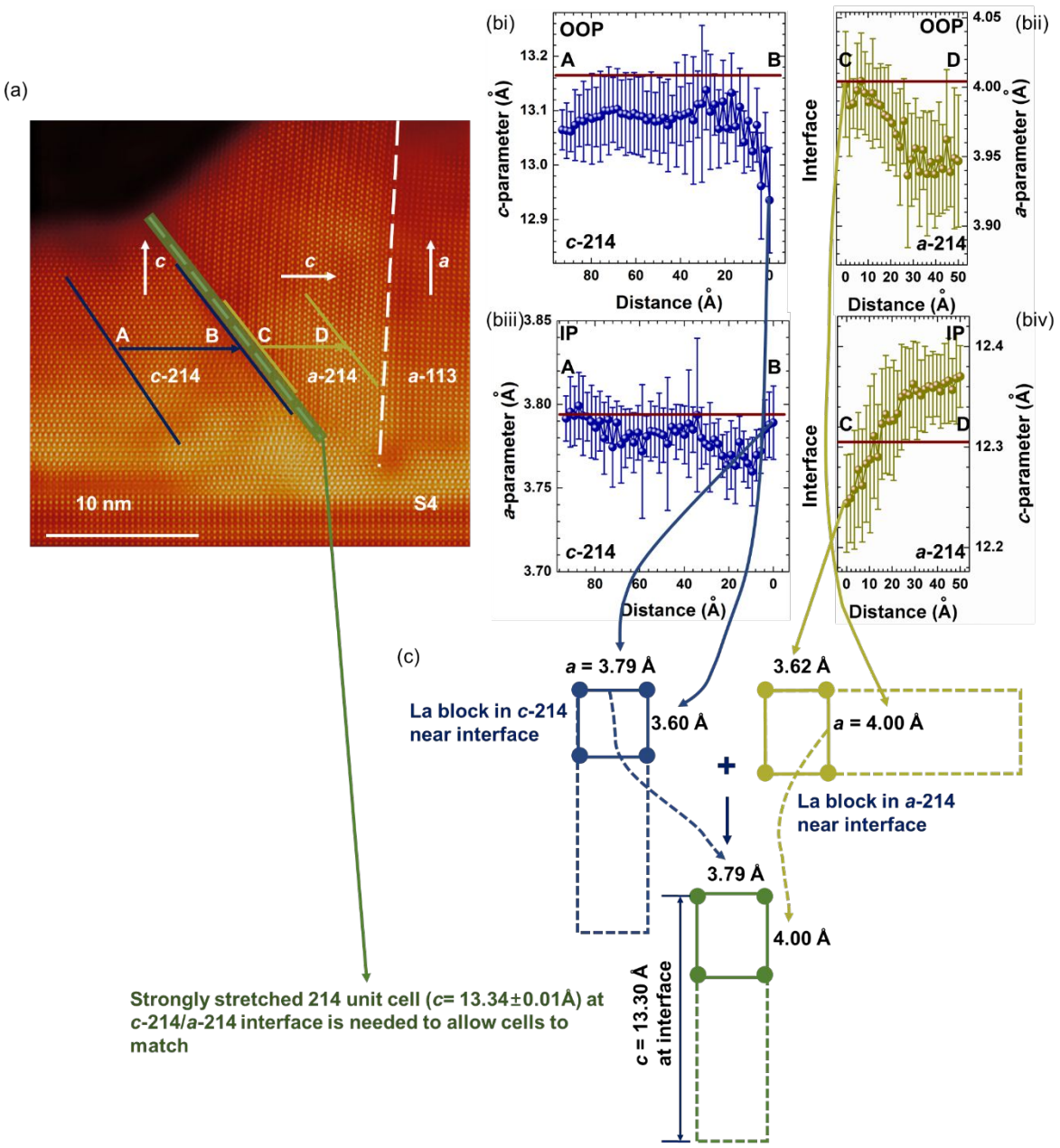

Fig. 5. Interfacial structure and strain model showing distortion of the shared La block at the (103) boundary between *c*-214 and *a*-214. (a) STEM image shows the *c*-214/*a*-214 interfacial region, with lines A-B and C-D drawn indicating the regions where lattice

parameter analyses were undertaken. (b) Measured lattice parameters on either side of the (103) boundary. *c*- and *a*-parameters in, respectively, the *c*-214 and *a*-214 grains. *c*-parameters shown in i and iv, and *a*-parameters shown in ii and iii. The lattice parameter analysis was undertaken horizontally from left and right on both sides of the *c*-214/*a*-214 interface. The bars represent the variation in vertical lattice parameters (over ~150 Å) along the length of lines that run parallel to the interfaces (i.e. ~45° w.r.t the substrate plane). The brown solid lines indicate the lattice parameters of bulk 214 and bulk T'214. (c) Measured lattice parameters in La blocks in *c*-214 and in *a*-214 respectively, which lie just to the left and right of the interfaces, and model proposed for shared La block between *c*-214 and *a*-124 right at the interface (central lower image).

The first observation from the lattice parameter analysis is that neither the *c*- nor the *a*-parameters in *c*-214 (Fig. 5(bi) and (biii), respectively) are increased compared to the bulk and so the observed structural deformation *within c*-214 cannot explain the T_C of 120 K. As would be expected, *within* each grain on either side of the boundary, the lattice parameters strain elastically, i.e. when *c* in *c*-214 (Fig. 5(bi)) decreases near the

interface, *a* in *c*-214 (Fig. 5(biii)) increases. Likewise, when *a* increases in *a*-214 (Fig. 5(bii)), *c* decreases (Fig. 5(biv)).

The second observation is that as the interface is approached, the lattices of both phases diverge from the bulk, presumably to achieve the lowest level of interfacial strain. It is important to note again that the boundary direction is along (103) and so to minimize strain, the La blocks at the top of the 214 unit cells in the *c*-214 and *a*-214 grains (as shown in Fig. 3(g)) must distort to match one another along the (103) plane.

The question now is *how* the La blocks can distort to match one another right at the (103) interface. To determine this, we need to first understand the distortions in the La blocks in *c*-214 and *a*-214 just to the left and right hand side of the interface. The OOP and IP values of the La blocks were measured using distances between atomic columns, using a 2-D Gaussian fitting. Just to the left of the (103) interface, the La block in *c*-214 (left hand image of Fig. 5(c)), has an IP La-La length of 3.79 ± 0.01 Å (from Fig. 5(biii)) and an OOP La-La length of 3.60 ± 0.01 Å (this is a fraction of the interfacial *c* value of Fig. 5(bi)). Just to the right of the interface, the La block in *a*-214 has an OOP

La-La length of 4.00 ± 0.01 Å (from Fig. 5(bii)) and IP La-La length of 3.62 ± 0.01 Å (a fraction of the interfacial *c* value, of Fig. 5(biv)).

The shared La blocks right at the interface, will *not* have dimensions that are simply an average of the two shared cells on either side of the boundary. This is because there is a very large anisotropy of the grain shapes, the *c*-214 grains being very wide relative to their height and vice versa for the *a*-214 grains. Therefore, because a much larger force will be exerted by the very large number of atoms in the wide *a* plane in the *c*-214 grains than from the much smaller number of atoms in the much thinner *a* direction in the *a*-214 grains, then the La-La distance in the IP direction in the interfacial block will remain fixed to the value in the *c*-214 grains (~ 3.79 ± 0.01 Å) The same argument holds true for the control of the La-La distance in the OOP direction, i.e. the La-La distance will be controlled by the *a*-214 grains, and hence will be fixed to the 4.00 ± 0.01 Å interfacial value. A further factor which will ensure the IP La-La distance is controlled by *c*-214 grains and the OOP La-La distance by the *a*-214 grains is that 214 has a layered structure in which there is no connectivity of the $LaCuO_3$ perovskite along the

OOP direction. Hence, distortion of the structure is much easier OOP than IP. This will mean that the shared La block at the interface will maintain the IP lattice parameters of the block on either side of the interface. According to our model, the shared La block (central lower image of Fig. 5(c)) has, in the 2-D plane, dimensions of 3.79 ± 0.01 Å IP × 4.00 ± 0.01 Å OOP. These La block dimensions translate to *a*- and *c*-parameters of 3.79 ± 0.01 Å and 13.34 ± 0.01 Å in the *c*-214 u.c., right at the interface.

We note that a T_C of 120 K has been observed previously in a single layer cuprate system, $HgBa_2CuO_{4+\delta}$ (Hg-1201), under hydrostatic pressure [41]. 120 K is the highest T_C so far observed for single layer cuprates. To achieve even higher T_Cs in single layer cuprates, optimum Cu-O distances are required *both* IP and OOP. Currently, these distances do not appear to optimize together in either the 214 films or the Hg-1201 under pressure. Considering Hg-1201 first, under ambient conditions, Hg-1201 has a T_C of 85 K, higher than bulk 214 where T_C is 40 K, and its apical oxygen distance is 2.8 Å compared to 2.4 Å for bulk 214 [19]. This explains the higher T_C since T_C correlates

directly with the apical distance [20]. At the same time, however the *a* parameter for Hg-1201 is only 3.884 Å which is above the ideal 3.84 Å value for optimum pairing [22,42–44].

When under pressure, the Hg-1201 *a*-parameter is near to the optimal value of 3.84 Å. However, the apical distance is compressed [44]. The optimum *a* parameter explains the increase in T_C from 85K to 120 K, even though the apical distance is reduced.

Considering now our strained *c*-214 at the (103) interface with *a*-214, an *a*-parameter below this optimal value, at 3.79 ± 0.01 Å, was obtained, but this is compensated by the much extended *c*-parameter, which is calculated to be 13.34Å ± 0.01Å (Fig. 5)[41], and which is consistent with an increased apical distance also.

It may be possible that an even higher T_C could be obtained in single layer cuprates if *both* apical distance were stretched and *a* were optimized to be close to 3.84 Å, which they don't appear to be in either our strained c-124 or in Hg-1201 under pressure. Achieving an optimized *a*-parameter in c-214 should be possible by coherent growth of composite 214 films on a structurally matched substrate with lattice parameters close to

3.84 Å. Finally, there is also the possibility to explore strain engineering of the (103) planes in 214 by growing artificial superlattices of this orientation.

Conclusions

In vertically aligned nanocomposite (VAN) thin films of $La_2CuO_{4+\delta}$ + $LaCuO_3$ grown on (001) STO, in a number of samples weak magnetic signatures of superconductivity up to 120 K were observed. This occurred *only* when *a*-axis oriented 214 (*a*-214) was present in the films, *in addition to* the main *c*-214 phase. The signatures are consistent with the observation of very high quality, highly strained interfacial regions in c-214 at (103) *c*-214/*a*-214 interfaces. A model in presented in which strongly distorted La perovskite blocks are formed in *c*-214 at the interfaces, which fits the extended Cu-O_A distances measured. The 120K T_C value is equal to the maximum value obtained previously in the single layer cuprate, $HgBa_2CuO_{4+\delta}$, formed under pressure [41].

Conflicts of interest

There are no conflicts to declare.

Author Contributions

This work was designed by J.L.M-D. E.M.C. and J.F. fabricated and characterized the films. E.M.C. measured the superconductivity. B.Z and P.L. processed and analyzed STEM data. P.L. performed STEM characterization. X.S. and H.W. performed TEM characterization. The manuscript was written by J.L.M-D and E.M.C. with contributions of all authors. All authors have given approval to the final version of the manuscript.

Acknowledgment

J.L.M-D and E.-M.C. thank the Isaac Newton Trust in Cambridge (minute 16.24(p)). J.L.M-D and J.F acknowledge the Engineering and Physical Sciences Research Council, Doctoral training account (grant number EP/N509620/1) for funding. B.Z. acknowledges funding from the China Scholarship Council and Cambridge Commonwealth, European and International Trust. Sandia National Laboratories is a multi-program laboratory managed and operated by National Technology and Engineering Solutions of Sandia, LLC., a wholly owned subsidiary of Honeywell International, Inc., for the U.S. Department of Energy's National Nuclear Security

Administration under contract DE-NA0003525. H.W. and X. S. acknowledge the support from the U.S. National Science Foundation (DMR-1565822) for the TEM effort at Purdue.

References

1 R. Hord, G. Cordier, K. Hofmann, A. Buckow, G. Pascua, H. Luetkens, L. Alff and B. Albert, *Zeitschrift fur Anorg. und Allg. Chemie*, 2011, **637**, 1114–1117.

2 K. Fujita, T. Noda, K. M. Kojima, H. Eisaki and S. Uchida, *Phys. Rev. Lett.*, 2005, **95**, 1–4.

3 J. A. Attfield, J. P., Kharlanov, A. L. & McAllister, *Nature*, 1998, **394**, 157–159.

4 W. B. Gao, Q. Q. Liu, L. X. Yang, Y. Yu, F. Y. Li, C. Q. Jin and S. Uchida, *Phys. Rev. B*, 2009, **80**, 094523.

5 Y. E. Suyolcu, Y. Wang, F. Baiutti, A. Al-Temimy, G. Gregori, G. Cristiani, W. Sigle, J. Maier, P. A. Van Aken and G. Logvenov, *Sci. Rep.*, 2017, **7**, 453.

6 F. Baiutti, G. Logvenov, G. Gregori, G. Cristiani, Y. Wang, W. Sigle, P. A. Van Aken and J. Maier, *Nat. Commun.*, 2015, **6**, 8586.

7 F. Baiutti, G. Gregori, Y. Wang, Y. E. Suyolcu, G. Cristiani, P. A. Van Aken, J. Maier and G. Logvenov, *ACS Appl. Mater. Interfaces*, 2016, **8**, 27368–27375.

8 L.-P. Locquet, J. Perret, J. Fompeyrine, E. Machler, J. W. Seo and G. Van Tendeloo, *Nature*, 1998, **453–456**, 141–144.

9 L. Forra, V. Ilakovac and B. Keszei, *Phys. Rev. B*, 1990, **41**, 9551–9554.

10 X.-J. Chen, V. V. Struzhkin, R. J. Hemley, H. Mao and C. Kendziora, *Phys. Rev. B*, 2004, **70**, 214502.

11 F. Nakamura, M. Kodama, S. Sakita, Y. Maeno and T. Fujita, *Phys. Rev. B*, 1996, **54**, 61–64.

12 F. Nakamura, T. Goko, J. Hori, Y. Uno, N. Kikugawa and T. Fujita, *Phys. Rev. B*, 2000, **61**, 107–110.

13 A. Gozar, G. Logvenov, L. F. Kourkoutis, A. T. Bollinger, L. A. Giannuzzi, D. A. Muller and I. Bozovic, *Nature*, 2008, **455**, 782–785.

14 V. Y. Butko, G. Logvenov, N. Božović, Z. Radović and I. Božović, *Adv. Mater.*, 2009, **21**, 3644–3648.

15 H. Zhou, Y. Yacoby, V. Y. Butko, G. Logvenov, I. Bozovic and R. Pindak, *Proc. Natl. Acad. Sci.*, 2010, **107**, 8103–8107.

16 E. Pavarini, I. Dasgupta, T. Saha-Dasgupta, O. Jepsen and O. K. Andersen, *Phys. Rev. Lett.*, 2001, **87**, 47003-1-47003–4.

17 F. C. Zhang and T. M. Rice, *Phys. Rev. B*, 1988, **37**, 3759–3761.

18 Y. Ohta, T. Tohyama and S. Maekawa, *Phys. Rev. B*, 1991, **43**, 2968–2982.

19 H. Sakakibara, H. Usui, K. Kuroki, R. Arita and H. Aoki, *Phys. Rev. Lett.*, 2010, **105**, 2–5.

20 D. J. Scalapino, *Rev. Mod. Phys.*, 2012, **84**, 1383–1417.

21 J. He, R. F. Klie, G. Logvenov, I. Bozovic and Y. Zhu, *J. Appl. Phys.*, 2007, **101**, 073906.

22 C. N. R. Rao and A. K. Ganguli, *Chem. Soc. Rev*, 1995, **24**, 1–7.

23 C. Gadermaier, V. V. Kabanov, A. S. Alexandrov, L. Stojchevska, T. Mertelj, C. Manzoni, G. Cerullo, N. D. Zhigadlo, J. Karpinski, Y. Q. Cai, X. Yao, Y. Toda, M. Oda, S. Sugai and D. Mihailovic, *Phys. Rev. X*, 2014, **4**, 1–6.

24 A. Bianconi, S. Agrestini, G. Bianconi, D. Di Castro and N. L. Saini, *J. Alloys Compd.*, 2001, **317–318**, 537–541.

25 S. Tan, Y. Zhang, M. Xia, Z. Ye, F. Chen, X. Xie, R. Peng, D. Xu, Q. Fan, H. Xu, J. Jiang, T. Zhang, X. Lai, T. Xiang, J. Hu, B. Xie and D. Feng, *Nat. Mater.*, 2013, **12**, 634–640.

26 S. He, J. He, W. Zhang, L. Zhao, D. Liu, X. Liu, D. Mou, Y. B. Ou, Q. Y. Wang, Z. Li, L. Wang, Y. Peng, Y. Liu, C. Chen, L. Yu, G. Liu, X. Dong, J. Zhang, C. Chen, Z. Xu, X. Chen, X. Ma, Q. Xue and X. J. Zhou, *Nat. Mater.*, 2013, **12**, 605–610.

27 J. F. Ge, Z. L. Liu, C. Liu, C. L. Gao, D. Qian, Q. K. Xue, Y. Liu and J. F. Jia, *Nat. Mater.*, 2015, **14**, 285–289.

28 M. Karppinen, H. Yamauchi, H. Suematsu, K. Isawa, M. Nagano, R. Itti and O. Fukunaga, *J. Solid State Chem.*, 1997, **222**, 213–222.

29 J. F. Bringley, B. A. Scott, S. J. La Placa, T. R. Mcguire and F. Mehran, *Phys. Rev. B*, 1993, **47**, 15269–15275.

30 J. F. Bringley, B. A. Scott, S. J. La Placa, R. F. Boehme, T. M. Shaw, M. W. McElfresh, S. S. Trail and D. E. Cox, *Nature*, 1990, **347**, 263–265.

31 E.-M. Choi, A. Di Bernardo, B. Zhu, P. Lu, H. Alpern, K. H. L. Zhang, T. Shapira, J. Feighan, X. Sun, J. Robinson, Y. Paltiel, O. Millo, H. Wang, Q. Jia and J. L. MacManus-Driscoll, *Sci. Adv.*, 2019, **5**, eaav5532.

32 I. MacLaren, M. Nord, P. E. Vullum, T. Tybell and R. Holmestad, *Adv. Struct. Chem. Imaging*, , DOI:10.1186/s40679-017-0042-5.

33 T. L. Meyer, L. Jiang, S. Park, T. Egami and H. N. Lee, *APL Mater.*, 2015, **3**, 126102.

34 I. E. Trofimov, L. A. Johnson, K. V. Ramanujachary, S. Guha, M. G. Harrison, M. Greenblatt, M. Z. Cieplak and P. Lindenfeld, *Appl. Phys. Lett.*, 1994, **65**, 2481.

35 M. Truchlý, T. Plecenik, O. Krško, M. Gregor, L. Satrapinskyy, T. Roch, B. Grančič, M. Mikula, A. Dujavová, Š. Chromik, P. Kúš and A. Plecenik, *Phys. C Supercond. its Appl.*, 2012, **483**, 61–66.

36 D. Lee and H. N. Lee, *Materials (Basel).*, 2017, **10**, 1–22.

37 A. Tsukada, T. Greibe and M. Naito, *Phys. Rev. B - Condens. Matter Mater. Phys.*, 2002, **66**, 1845151–1845155.

38 M. I. Houchati, M. Ceretti, C. Ritter and W. Paulus, *Chem. Mater.*, 2012, **24**, 3811–3815.

39 F. C. Chou, J. H. Cho, L. L. Miller and D. C. Johnston, *Phys. Rev. B*, 1990, **42**, 6172–6180.

40 Y. Imai, M. Kato, Y. Takarabe, T. Noji and Y. Koike, *Chem. Mater.*, 2007, **19**, 3584–3585.

41 L. Gao, Y. Y. Xue, Q. Xiong, R. L. Meng, D. Ramirez and C. W. Chu, *Phys. Rev. B*, 1994, **50**, 4260–4263.

42 E. V. Antipov, A. M. Abakumov and S. N. Putilin, *Supercond. Sci. Technol.*, , DOI:10.1088/0953-2048/15/7/201.

43 B. A. Hunter, J. D. Jorgensen, J. L. Wagner, P. G. Radaelli, D. G. Hinks, H. Shaked, R. L. Hitterman and R. B. Von Dreele, *Phys. C Supercond. its Appl.*, 1994, 221, 1–10.

44 A. M. Balagurov, D. V. Sheptyakov, V. L. Aksenov, E. V. Antipov, S. N. Putilin, P. G. Radaelli and M. Marezio, *Phys. Rev. B*, 1999, **59**, 7209–7215.